Physics of the Earth and Planetary Interiors 261 (2016) 133–140

Contents lists available at ScienceDirect

Physics of the Earth and Planetary Interiors

journal homepage: www.elsevier.com/locate/pepi

Near-field radiated wave field may help to understand the style of the supershear transition of dynamic ruptures

Andrea Bizzarri [a,*], Chao Liu [b]

[a] Istituto Nazionale di Geofisica e Vulcanologia, Sezione di Bologna, Via Donato Creti, 12, 40128 Bologna, Italy
[b] Department of Earth Sciences, University of Oxford, South Parks Road, OX1 3AN Oxford, UK

ARTICLE INFO

Article history:
Received 28 September 2015
Received in revised form 24 May 2016
Accepted 24 May 2016
Available online 30 May 2016

Keywords:
Supershear earthquakes
Ground motions
Wave propagation
Dynamic models of faults
Computational seismology

ABSTRACT

Supershear earthquakes are known to leave special signatures in the signals on the fault (fault slip velocity, dynamic traction evolution, energy flux, etc.) and in the ground motions. Moreover, two different styles of supershear transition have been identified; in the direct transition (DT) mechanism the rupture speed continuously increases from the sub-Rayleigh to the terminal speed of *P* waves, while in the mother–daughter (MD) mechanism a forbidden zone of rupture speed exists and a secondary pseudo-rupture is generated ahead of the primary rupture front. Here we found that the off-fault signals (wave-fields) generated by these two mechanisms are rather different, in that the MD case contains an enhanced trailing Rayleigh field, which has very low amplitudes (or it is even practically absent) in the DT case, and possess higher frequency content. Therefore, we show that it is possible to distinguish the style of the supershear transition from the records of real earthquakes. In particular, basing on the results of our numerical simulations, we can conclude that the Denali, Alaska, earthquake was basically controlled by a classical MD mechanism.

1. Introduction

It is well known that supershear earthquakes (namely, dynamic ruptures propagating with a rupture speed greater than that of the *S* waves of the medium surrounding the seismic source, v_S) possess some features that differentiate them from subshear events. Indeed, supershear earthquakes emit a Mach cone which is fully coherent at some distance from the fault (Bernard and Baumont, 2005) and which has enhanced high frequencies that can overwhelm those arising from stress heterogeneity (Spudich and Frazer, 1984; Bernard and Baumont, 2005; Bizzarri et al., 2010). Moreover, they can radiate a wave front having less geometric spreading than that radiated from subshear events (Bernard and Baumont, 2005; Bizzarri and Spudich, 2008). They also emit Rayleigh Mach waves which do not attenuate with distance from the fault trace (Dunham and Bhat, 2008). Additionally, ground motions of supershear events are richer in high frequencies (Bizzarri et al., 2010) and they extend widely in the direction perpendicular to the fault trace, with a predominance of the fault-parallel component of the particle velocity (Aagaard and Heaton, 2004). Finally, supershear earthquakes tend to enhance rake rotation (Bizzarri and Cocco, 2005; Bizzarri and Das, 2012); this can have consequences in the formulation of analytical expression of the slip-dependent constitutive models (Bizzarri, 2014b). All these features have relevant practical implications and this is the reason of an increasing interest in studying supershear earthquakes and, in general, to infer the rupture speed of dynamic events (Das, 2007). An up-to-date list of real-world earthquakes that have been identified as supershear can be found in Bizzarri (2014; his Table I). Indeed, there are also some attempts to relate supershear events to seismic hazard (e.g., Andrews, 2010 among others).

Within the range of supershear rupture speeds, there are two rather different supershear transition mechanisms (Geubelle and Kubair, 2001; Liu et al., 2014; see also Festa and Vilotte, 2006); one is the direct transition (DT thereinafter) and the other one is the mother–daughter (MD thereinafter) transition (see also Dunham, 2007; Liu and Lapusta, 2008; Lu et al., 2009). In particular, Liu et al. (2014) found that for weak faults (namely, for relatively small values of the strength parameter S ($\sim 0.38 \leqslant S \leqslant \sim 0.72$)) the ruptures penetrate the previously considered forbidden zone of rupture speed (between Rayleigh speed, v_R, and v_S) through the direct transition mechanism. As well known, $S \underset{\text{df}}{=} \frac{\tau_u - \tau_0}{\tau_0 - \tau_f} = \frac{\Delta\tau_0}{\Delta\tau_d}$ expresses the degree of instability of a fault, in that a low value of S identifies an unstable fault, over which a rupture

* Corresponding author. Tel.: +39 051 4151432; fax: +39 051 4151499.
E-mail addresses: andrea.bizzarri@ingv.it (A. Bizzarri), Chao.Liu@earth.ox.ac.uk (C. Liu).

http://dx.doi.org/10.1016/j.pepi.2016.05.013
0031-9201/

with relevant stress drop is expected. The strength parameter, which in fact is the ratio between the strength excess and the dynamic stress drop, has been first introduced by Das and Aki (1977a,b). The importance of the S parameter resides in the fact that it discriminates between supershear and sub-Rayleigh propagation regimes, depending of the fact that the value of S is below or above, respectively, a critical value, which in turn depends on the dimensionality of the problem (2-D or 3-D problem; see Dunham, 2007). Indeed, the rupture speed (v_r, the measure of the velocity at which the rupture propagates on the fault surface) continuously increases from sub-Rayleigh speeds to the terminal speed of P waves, v_P, without any jump, contrarily to the previous believe from Andrews (1976); the rupture crosses the forbidden and the unstable zones through a rapid acceleration. In this case, the energy flux at the rupture front undergoes a sharp but monotonic increase, including the velocity range $v_R < v_r < v_S$ (Bizzarri, 2013) that is forbidden in the 2-D, steady-state, singular cracks (Broberg, 1999). On the other hand, for stronger faults (namely, when $\sim 0.76 \leqslant S \leqslant \sim 1.3$) there is a peak in the shear stress field (i.e., a stress concentration) which travels ahead of the main (mother) rupture front and causes the birth of a secondary (daughter) pseudo-rupture is ahead of mother front. While the latter asymptotically approaches v_R, the former starts to propagate already in the supershear regime and finally can reach v_P. In this case, the MD mechanism, the forbidden zone does really exist and the rupture speed experiences a jump from the sub-Rayleigh regime to the supershear one. Correspondingly, the energy flux at the rupture front exhibits a sharp peak during the coalescence of the main and the daughter rupture fronts (Geubelle and Kubair, 2001). This MD regime has been explored in the above-mentioned, pioneering paper by Andrews (1976)—S was 0.8 in that case; see his Fig. 3—and in fact becomes the epitome of the supershear rupture propagation. Indeed, the large (nearly complete, with the very few, recent exceptions mentioned above) subsequent literature on this subject assumed that the MD mechanism was the unique behavior of supershear ruptures.

The distinction between these two styles has been obtained by computing the rupture speed v_r and looking whether it fails within the forbidden zone (as for the DT mechanism) or not (as for the MD mechanism). v_r is computed by using the two-points central difference scheme, in which in the fault node i is expressed as it follows:

$$v_r(i) = \frac{2\Delta x}{t_r(i+1) - t_r(i-1)} \tag{1}$$

where Δx is the spatial sampling (i.e., the discretization along the direction of the propagation of the rupture) and t_r is the rupture time of the node i, which in turn is defined as the first instant at which the fault slip velocity in i exceeds the threshold value of v_l = 0.01 m/s (Bizzarri and Das, 2012). Moreover, the distinction between the two styles of supershear transition has been also made by looking whether the cohesive zone (where the stress is released on the fault) exhibits its so-called bifurcation, i.e., if there is the birth of a secondary (daughter) rupture front ahead from the primary (or mother) front. Due to the numerical nature of the problem, it is virtually impossible to find an *exact*, *arbitrarily accurate* value which distinguishes the two regimes, and this is the reason why Liu et al. (2014) gave the value "$\sim$0.72" as upper bound for S in the DT mechanism and the value of "$\sim$0.76" as lower bound for the MD mechanism.

Since the styles of the supershear transition (DT and MD mechanisms) have rather different signatures on the fault surface, as elucidated by Liu et al. (2014), it is natural to ask whether the off-fault behavior is also different, i.e., whether the signals recorded out of the fault contain some special features and can therefore be used to infer what kind of transition mechanism is operating on a fault. This is the main goal of the present study.

2. Method

We solve the elastodynamic problem for a 2-D, pure in-plane (mode II) fault geometry and always including inertia. Namely, we solve the fundamental elastodynamic equation for faults (i.e., the Newton's second law of dynamic for rigid bodies), which, neglecting body forces (such as electric and magnetic forces, gravity, etc.), reads

$$\rho \ddot{u}_i = \sigma_{ij,j} \tag{2}$$

in which ρ is the cubic mass density of the medium surrounding the fault, $\mathbf{u}$ is the fault slip (formally, the displacement discontinuity), σ_{ij} are the stress tensor components and repeated index are summated (Einstein's convention assumed). Eq. (2) is solved numerically, as described in details in Bizzarri et al. (2001) and in Liu et al. (2014). Here we simply recall that the problem is solved by using a second-order accurate, finite difference scheme, based on triangular grid, with homogeneous mesh. The code is OpenMP-parallelized. The nucleation is imposed in an initialization patch (exactly as in Liu et al., 2014; their Section 2) and then the rupture propagates spontaneously (i.e., without prior-assigned rupture speed) along x_1 (see Fig. 1). For the mode II geometry assumed here, the fault slip is then $((u_1(x_1,t)),0,0)$, since no opening or interpenetration of material is allowed and the solutions only depend, by definition, on the x_1 coordinate. The fault is governed by the classical slip-weakening law, which prescribes a linear decrease of the fault friction with increasing fault slip over the prescribed, characteristic distance d_0:

$$\tau = \begin{cases} \left[\mu_u - (\mu_u - \mu_f)\frac{u}{d_0}\right]\sigma_n^{eff} & , u < d_0 \\ \mu_f \sigma_n^{eff} & , u \geqslant d_0 \end{cases} \tag{3}$$

In Eq. (3) $\mu_u \sigma_n^{eff} = \tau_u$ is the upper yield stress and $\mu_f \sigma_n^{eff} = \tau_f$ is the residual level (σ_n^{eff} is the effective normal stress, which is assumed to be constant through time in the present work). We

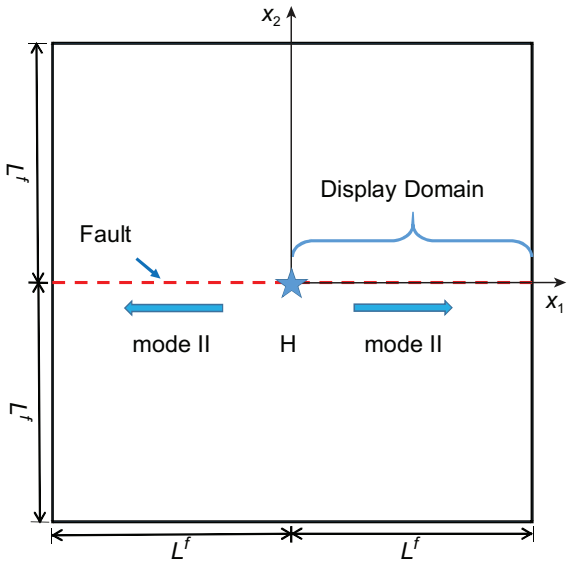

Fig. 1. Geometry of the fault considered in the present study. The dashed line indicates the fault trace. The rupture nucleates at the (imposed) hypocenter H and then propagates bilaterally and spontaneously. Due to the symmetry of the problem, only one half of the fault is considered (as indicated).

are aware that this fault governing model is a mere idealization of the truly complexity of a real-world fault (see Bizzarri, 2011, 2014a), but we prefer to start with this simple constitutive equation. The results can be then generalized to other governing models, including a more complicated (and perhaps realistic) behavior of the fault friction within the coseismic time scale. All the frictional properties are homogeneous for sake of simplicity and the model parameters are exactly those of Liu et al. (2014); they are recalled for completeness in Table 1. The spatio-temporal discretization adopted in the numerical experiments presented here ($\Delta x = 40$ m, $\Delta t = 3.42 \times 10^{-4}$ s) ensures a proper resolution of the cohesive zone (where the stress drops from τ_u to τ_f over the distance d_0) and of the rupture speed (see Appendix A of Liu et al., 2014 for a thorough discussion on the numerical details). The rupture propagation (and the consequent stress redistribution) on the fault induces elastic deformations (and thus displacement) in the Hookean, Poissonian and homogeneous medium surrounding the fault. As stated above, due to the geometry of the problem we do not have any dependence on the depth (i.e., on the x_3 coordinate), so that the particle displacement and their time derivative (**U** and **V**, respectively) possess a spatial dependence only on x_1 and on x_2 (strike and off-fault coordinates, respectively). In the remained of the paper we will refer to $V_1(x_1, x_2, t)$ and to $V_2(x_1, x_2, t)$ as the fault-parallel (FP henceforth) and the fault-normal (FN henceforth) component of the particle velocity fields, respectively. Moreover, we freely speak of "ground motions" although, namely, there is no the free-of-traction condition in the present model. Indeed, we know that the Mach cone originated by the supershear rupture propagation does not depends on the presence of the free surface (see, e.g., Dunham and Bhat, 2008; their Fig. 1); the latter is known only to produce the additional Rayleigh-Mach waves (Dunham and Bhat, 2008; Bizzarri et al., 2010) and it tends to enhance the supershear propagation once the rupture front interacts with it (Olsen et al., 1997; Chen and Zhang, 2006; Zhang and Chen, 2006; Day et al., 2008; Bizzarri, 2010; Kaneko and Lapusta, 2010; Bizzarri and Das, 2012; Zhang et al., 2014).

3. Ground motions of supershear earthquakes

Among the different numerical experiments performed we selected two cases, both failing in the supershear regime and which are fully representative of the two different transition classes. We remark here that these two models are not *extreme* examples of the two regimes, but, as stated, quite representative, in that they clearly exhibit the differences pertaining to the two different styles of supershear transition. While Model A has the strength parameter $S = 0.4$, Model B has $S = 0.9$; both the configurations have the same initial shear stress τ_0 and the same τ_f (so that the dynamic stress drop is also the same; $\Delta\tau_d = \tau_0 - \tau_f = 18.6$ MPa). In such a way the amplitudes of the ground velocity of Models A and B reported in the following are directly comparable. However, the former has $\tau_u = 81.24$ MPa (which corresponds to an upper friction coefficient $\mu_u = 0.677$), while the latter has $\tau_u = 90.54$ MPa ($\mu_u = 0.755$). As depicted in Fig. 2 of Liu et al. (2014), Model A is representative of the DT mechanism and Model B of the MD mechanism.

Table 1
Reference parameters adopted in the numerical simulations presented and discussed in this study. We consider homogeneous properties and a constant effective normal stress.

Parameter	Value
Lamé' s constants, $\lambda = G$	35.9 GPa
S wave speed, v_S	3.464 km/s
Rayleigh speed, v_R	3.184 km/s
Eshelby speed, $v_E = \sqrt{2}v_s$	4.899 km/s
P wave speed, v_P	6 km/s
Effective normal stress, σ_n^{eff}	120 MPa
Initial shear stress (pre-stress), τ_0	73.8 MPa
Dynamic friction coefficient, μ_f	0.46
Dynamic friction level, τ_f	55.2 MPa
Dynamic stress drop, $\tau_0 - \tau_f$	18.6 MPa
Characteristic slip-weakening distance, d_0	0.4 m

The snapshots of the spatial distribution of the particle velocity field in the whole medium are reported in Fig. 2. The movies of the entire dynamic evolution of the ruptures are available as Movies S1 and S2 of the Supporting information. As expected, we can clearly recognize the presence of the shear Mach (M_S) waves, that are generated by the two supershear ruptures. Shear Mach waves are preceded by a first peak in particle velocity (the arc denoted with the symbol P_1 in Fig. 2), which is associated with dilatational motion (Bizzarri et al., 2010). In general, we have that the M_S wavefront is more relevant at large distances from the fault for ruptures experiencing the DT mechanism with respect to those experiencing the MD mechanism. This is physically reasonable, because DT is characterized by a smaller value of the S parameter and thus by a higher level of fault instability (namely, since in our simulations τ_0 and τ_f are kept unchanged, Model A has a greater breakdown stress drop, $\Delta\tau_b$, and a greater fracture energy density, E_G; see Eqs. (12) and (18) of Bizzarri, 2011, respectively). This conclusion holds for both FP and FN components of particle velocity.

Remarkably, there is a more relevant difference between the wavefields of DT and MD mechanisms (the results discussed here are confirmed by other numerical simulations pertaining to the two regimes, not reported here for brevity). From Fig. 2 we see that in the MD mechanism it emerges another wavefield (the trailing Rayleigh field or trailing Rayleigh pulse), which has been first mentioned by Dunham and Archuleta (2004) in explaining the Denali, Alaska, PS10 record, has been experimentally identified by Mello et al. (2010, 2014). The trailing Rayleigh field does actually propagate at the Rayleigh wave speed, as one can infer from Movie S2, by considering the times and the locations of it. The trailing Rayleigh field is quite visible especially in the FN component of ground motions (see Fig. 2d); in the DT mechanism it is much lower (see Fig. 2b) and it is practically absent in the FP component (see Fig. 2a). The very small amplitude of the trailing Rayleigh field in the DT case is also confirmed by the results in a truly 3-D model (pertaining to a configuration with $S = 0.4$) by Bizzarri et al. (2010; see their Figs. 3a and c from 3rd to 5th snapshots).

From Fig. 2d, we can also see that in the MD case inside the shear Mach cone (i.e., at off-fault distances up to about 5 km for the time snapshot reported in Fig. 2d) the trailing Rayleigh field appears as a 8-shaped object in the FN component of **V**. This 8-shaped object is not vertical, but its lobes have a forward curvature, in total agreement with the results of Mello et al. (2010). This details are appreciable also from Movie S2. Far from the fault (namely, outside the shear Mach cone) the trailing Rayleigh field expands as an arcuate front, with a slightly lower curvature with respect to the P_1 arc.

In Fig. 3 we plot the particle velocity time histories at different stations located at a distance along strike of 20 km from the hypocenter. Data are low-passed at 8 Hz in order to avoid the numerical noise due to grid dispersion. These records clearly indicate the differences in the trailing Rayleigh field in the DT and in the MD models (top and bottom panels, respectively). While the trailing Rayleigh field is feebly recognizable in the case of DT, it is firmly seen in the case of MD. In the latter situation is amplitude is paramount with respect to that of M_S waves. Once the rupture propagates along the fault the trailing Rayleigh field expands and intersects the Mach cone and persists at large distance from the fault trace. As observed in Fig. 2d, also from Figs. 3c and d it emerges that for stations close to the fault trace (namely, inside the Mach cone) the behavior of the trailing Rayleigh field (marked

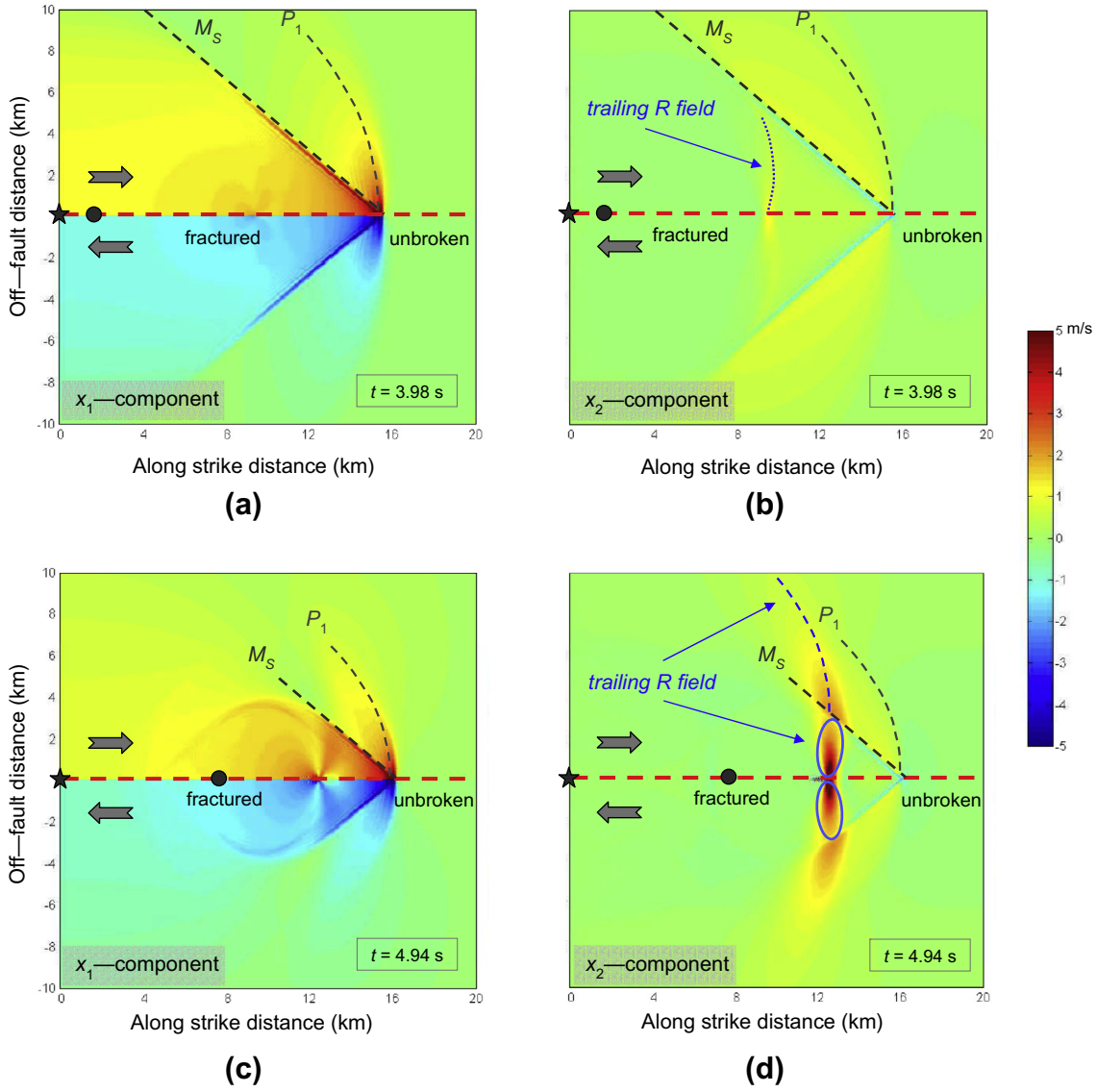

Fig. 2. Spatial distribution of the particle velocity fields from supershear ruptures. Top panels pertain to direct transition (DT) mechanism (S = 0.4, Model A), bottom panels pertain to mother–daughter (MD) mechanism (S = 0.9, Model B). Left panels report the fault-parallel (FP) component (namely, V_1), right panels report the fault-normal (FN) component (namely, V_2). In all panels the star indicates the imposed epicenter. The rupture propagates bilaterally (due to the symmetry of the problem, only the positive part of the x_1 axis is reported). The red dashed line denotes the fault trace and the big dots indicates the strike distances at which the supershear transitions occur (x_1 = 1.66 km for Model A and x_1 = 7.88 km for Model B, in agreement with Figs. 3b and 4b of Liu et al., 2014, respectively). The times of the snapshots (indicated in each panel) have been selected in order to have the same location of the rupture tip for both the models A and B. Big arrows emphasize the relative motion of the parts of the elastic medium separated by the fault interface. All relevant fields are also indicated (only in the positive x_2 half-plane, for better clarity). Trailing R field stands for the trailing Rayleigh field. (For interpretation of the references to colour in this figure legend, the reader is referred to the web version of this article.)

as dashed green lines in Fig. 3) has a forward curvature. Remarkably, this feature is observed also in the case of Model A (see Figs. 3a and b and, although the amplitude is significantly smaller, also in Fig. 2b). Incidentally, we remark here that since our models do not incorporate any stopping or self-healing mechanism (i.e., the rupture continues to propagate forever due to the homogeneities of the spatial distribution of the parameters), there is a permanent deformation in the x_1 direction, which corresponds to the fact that the particle velocity does not go back to zero.

The presence of the trailing Rayleigh field is also associated with a greater content in the high frequency; this is reported in Fig. 4. We compute the Fourier amplitude spectra (FAS) of the normalized particle velocity time histories at a receiver located at a distance of 20 km from the hypocenter (as in Fig. 3) and at an off-fault distance of 2 km. The normalization is done through the factor $G/(v_S\Delta\tau_d)$, G being the rigidity of the Poissonian medium. As in Bizzarri et al. (2010), we applied a half-cosine taper lasting 5 s to the seismograms (in the present case from 7 s to 12 s) in order to have final particle velocity equal to zero. Beyond the end of the tapered region, the seismograms were extended by adding zeros to the end such that all of the seismograms have the same total length. Due to numerical dispersion, the calculated spectra are only valid up to approximately 30 Hz, as indicated in Fig. 4. The frequency increment in the FAS is about 0.01 Hz. Notably, we can see from Fig. 4 that the spectral fall-off is rather similar in the two models and it falls in between ω^{-1} and ω^{-2}, as expected for supershear ruptures (see Bizzarri et al., 2010; ω being the frequency). In other words, the presence of the enhanced trailing Rayleigh field in the MD case is not able to alter the fall-off at high frequencies. However, we can also see that Model B (thin lines) tends to exhibit a slightly higher frequency content compared to Model A (thick lines), especially in the frequency band from 5 to 30 Hz.

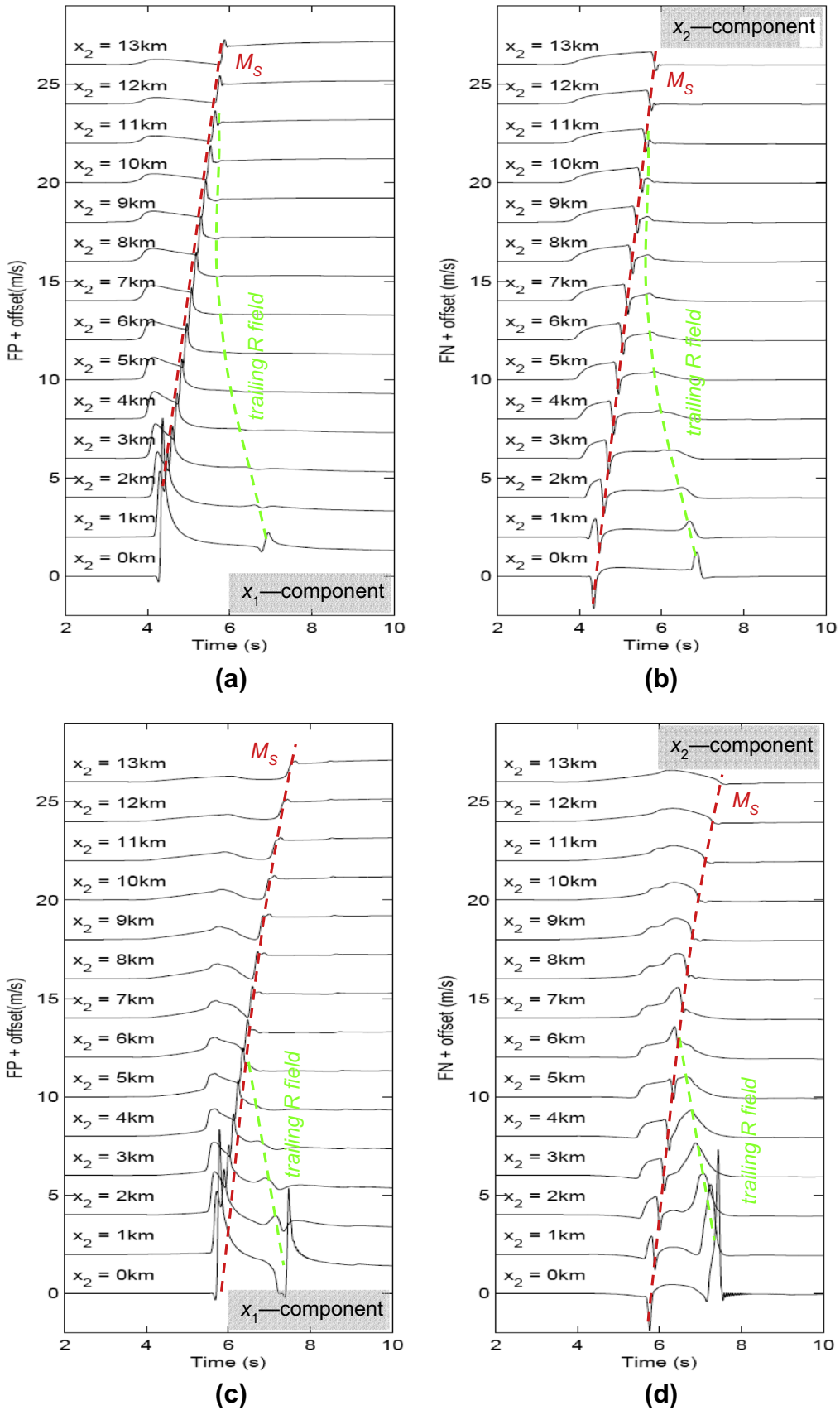

Fig. 3. Synthetic signals pertaining to the two models of Fig. 2 at a strike distance of 20 km from the hypocenter and for different off-fault distances (indicated near each trace). Again, top and bottom panels are for Model A and Model B, respectively; left and right panels report the FP and the FN component, respectively. Data are low-passed at 8 Hz and offset for nth receiver is $(n-1)$.

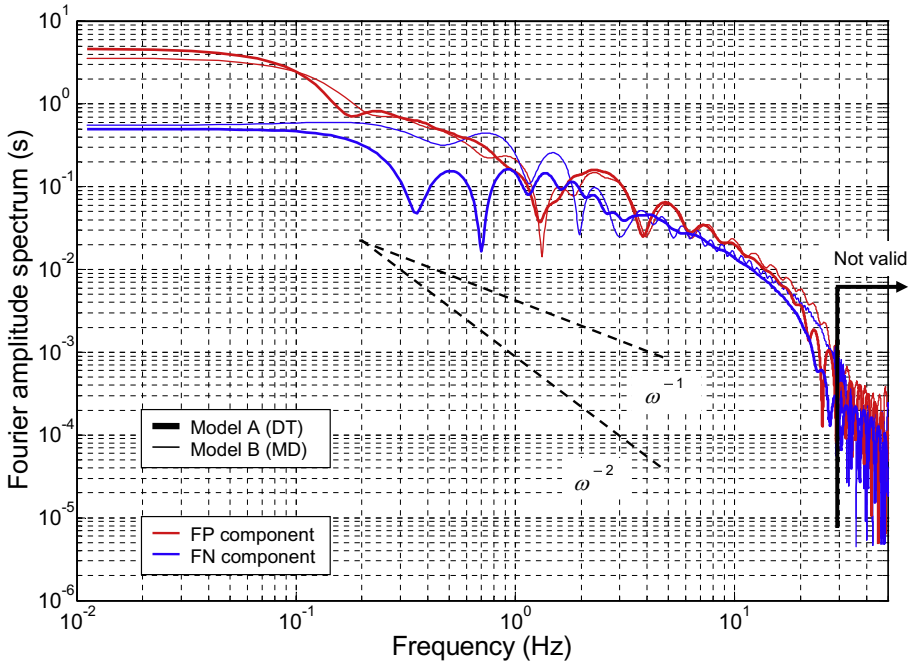

Fig. 4. Frequency amplitude spectrum (FAS) of the particle velocity time histories of Fig. 3 (data are normalized by the multiplier factor $G/(v_S \Delta\tau_d)$; G is the rigidity of the Poissonian medium). The selected receiver is at an off-fault distance of 2 km. Thick lines refer to Model A (DT mechanism), while thin lines refer to Model B (MD mechanism). Red and blue lines pertain to FP and FN component of **V**, respectively. FAS are computed as described in the text (see also Bizzarri et al., 2010; their Section 7). For frequencies greater than 30 Hz the results are affected by numerical oscillations (due to grid dispersion). (For interpretation of the references to colour in this figure legend, the reader is referred to the web version of this article.)

4. Conclusions and outlook

By scrutinizing the dynamic behavior of spontaneous, 2-D, pure mode II ruptures we found that the two kinds of the supershear transitions identified by previous studies (Geubelle and Kubair, 2001; Liu et al., 2014; see also Festa and Vilotte, 2006) have different signatures not only in the on-fault signals, but also in the radiated seismic waves (and thus in the ground motions). In the direct transition (DT) mechanism—typical of weak, very unstable faults ($\sim 0.38 \leqslant S \leqslant \sim 0.72$; S is the strength parameter), the rupture speed does penetrate the previously considered forbidden zone and continuously increases without any jump from sub-Rayleigh speeds to the terminal value of v_P. On the contrary, in the case of the mother–daughter (MD) mechanism—typical of stronger faults ($\sim 0.76 \leqslant S \leqslant \sim 1.3$)—the rupture speed experiences an abrupt jump from the sub-Rayleigh regime to the supershear one and the forbidden zone does really exist.

In the present paper we show that the two different supershear transition mechanisms cause systematic differences also in the off-fault behavior. Indeed, we demonstrate that the MD mechanism causes the birth of an enhanced trailing Rayleigh field, which is clearly visible especially in the fault-normal component of particle velocity. On the contrary this field is quite negligible (even if no absent) in the case of DT mechanism (see Figs. 2 and 3; see also Movies S1 and S2 of the Supporting information). In the MD case, the trailing Rayleigh field has an amplitude which even overcomes that of the shear Mach waves, in the fault-normal (FN) component of the particle velocity **V** (see Figs. 2d and 3d). Inside the Mach cone (i.e., close to the fault trace) the trailing Rayleigh field appears as a 8-shaped object, with the lobes that are slightly inclined and extend slightly out beyond the rupture. This forward curvature has been also observed in the numerical simulations by Mello et al. (2010; see their Fig. 10), where a station far of the fault is reached by that waves earlier with respect to a station close to the fault. Moreover, this effect is clearly observed and captured in photoelastic images of the laboratory experiment performed by Mello et al. (2010), showing the maximum shear stress field surrounding a sub-Rayleigh (or trailing sub-Rayleigh) rupture. In such cases the forward inclination of the field lobe is generally evident. In Fig. 23 of Mello et al. (2010) the behavior of the trailing Rayleigh field emerges from the relation of the point labeled as b_2 (which represents the time when the FN signal (recorded out of the fault trace) begins to dive and the time marker t_R which denotes the time of the rupture tip (i.e., the location of the rupture on the fault). It is important to remark that the trailing Rayleigh field remains a causal wave, in that it does not exceeds the P wave speed (it propagate with the velocity of v_R), as expected. Indeed, the causality condition (i.e., $\Delta x \geqslant v_P\ \Delta t$; Fukuyaman and Madariaga, 1998; Bizzarri et al., 2001) is numerically satisfied in all the experiments.

Our results also show that the spectral fall-off of DT and MD cases is rather similar and it falls in between ω^{-1} and ω^{-2} (see Fig. 4), as expected for supershear ruptures (see Bizzarri et al., 2010). However, the ground motions of the MD case possess a higher frequency content compared to the DT case. This can be due to the really enhanced high frequency of the pulse in the MD case or to the fact that in this situation there are two waves traveling.

The source of trailing Rayleigh field is two folded; (i) it is a concentrated stress perturbation that is a remnant of the mother (initially sub-Rayleigh) rupture (which in turn causes the birth of the supershear pseudo-rupture; Liu et al., 2014) and (ii) the breakdown process (i.e., the stress release) occurring at the supershear rupture tip should generate Rayleigh waves and hence nicely coalesce at the trailing Rayleigh field.

In the present paper we have compared two configurations to catch the main features of the two classes of supershear transition mechanisms. These two models are not extreme cases, but they the well represent the two regimes from which they belong and make it possible to clearly distinguish the differences existing between them. We are aware that the single details of the rupture behaviors (like the amplitudes of the particle velocity fields) depend on a lot of parameters, such as the governing parameters (τ_u, τ_0, τ_f and d_0), as

well as the elastic parameter of the medium. The most important point to be emphasized here is the presence of the trailing Raleigh field, which discriminates from DT and MD styles. Indeed, we highlight that as the parameter S varies in the two parameter regions discriminating between DT ($\sim 0.38 \leqslant S \leqslant \sim 0.72$) and MD supershear transition mechanism ($\sim 0.76 \leqslant S \leqslant \sim 1.3$) the main, overall characteristics of the wavefields will not change. Obviously, the amplitude of the 8-shaped object is reduced as long as the S parameter decreases toward the lower bound of the MD regime, so that the peaks in **V** close to the fault trace (those shown in Figs. 3c and d) are reduced. The general conclusions from the numerical experiments is that the DT mechanism the trailing Rayleigh field remains weak, while for the MD mechanism it remains strong.

The major outcome of the present study is that ground motions recorded far of the fault (i.e., seismograms) make it possible to distinguish not only between sub- and supershear ruptures (as already demonstrated elsewhere; see e.g. Dunham and Bhat, 2008; Bizzarri et al., 2010), but they are also able to discriminate between the two rather different styles of the supershear transitions, the DT and the MD mechanisms. Just for an example, numerical and laboratory results by Mello et al. (2014) indicate that the M 7.9 2002 Denali, Alaska earthquake exhibits the presence of a strong trailing Rayleigh field. Although it is beyond our present scope to produce (another) numerical model of the Denali earthquake and although the numerical experiments discussed here refer to idealized conditions (homogeneous properties, linear slip-weakening law, planar fault, etc.), our findings makes it possible to firmly conclude that the Denali rupture was basically dominated by the classical MD transition mechanism.

As a consequence of such an application of the findings of the present paper it would be natural to see whether they can be also applied to other real-world events, in order to discriminate the style of the supershear transition. Unfortunately, there are no clear evidences, at the moment, of other supershear earthquakes for which the presence of the trailing Rayleigh field has been recognized and indubitably identified. Indeed, the Denali earthquake is the finest example, as discussed by Mello et al. (2014). At a more fundamental level, we also mention here that the identification of the trailing Rayleigh field can be somehow complicated because of the presence of frictional heterogeneities in real-world events, which are expected to enrich (and complicate as well) the waves radiated from the source (see, e.g., Bizzarri et al., 2010 among others). Nevertheless, we aim that the discrimination we propose here can be applied in the future to other cases.

Finally, it is important to emphasize that there is no reason to believe that the two styles of the supershear transition (DT and MD mechanisms) and the related differences in the on-fault and off-fault behaviors (scrutinized by Liu et al., 2014 (see also Festa and Vilotte, 2006) and by the present work, respectively) are peculiar of the linear slip-weakening constitutive model. We can speculate that the only possible variation would appears in the value of the combination of governing parameters which discriminate between the two supershear transition mechanisms. Indeed, we emphasize that the presence of the forbidden zone in rupture speed has not been demonstrated for real earthquakes, but it has been only found in analytical studies and under special condition (namely, for 2-D, steady-state, singular cracks; Broberg, 1999) and as discussed by Kostrov and Das (1988) the rupture speed could be any value.

Acknowledgments

S. Das and R. Madariaga are greatly acknowledged for stimulating discussions on the topic. We also acknowledge M. Mello and H.S. Bhat for some general discussions about the trailing Rayleigh field and Eric M. Dunham for its causality. Finally, we thank two anonymous referee and the Associate Editor, Vernon Cormier, for useful comments which contribute to improve the paper. The data presented in this paper can be produced using the parameters mentioned above.

Appendix A. Supplementary data

Supplementary data associated with this article can be found, in the online version, at http://dx.doi.org/10.1016/j.pepi.2016.05.013.

References

Aagaard, B.T., Heaton, T.H., 2004. Near-source ground motions from simulations of sustained intersonic and supersonic fault ruptures. Bull. Seismol. Soc. Am. 94 (6), 2064–2078. http://dx.doi.org/10.1785/0120030249.

Andrews, D.J., 1976. Rupture velocity of plane strain shear cracks. J. Geophys. Res. 81, 5679–5687. http://dx.doi.org/10.1029/JB081i032p05679.

Andrews, D.J., 2010. Ground motion hazard from supershear rupture. Tectonophysics 439, 216–221. http://dx.doi.org/10.1016/j.tecto.2010.02.003.

Bernard, P., Baumont, D., 2005. Shear Mach wave characterization for kinematic fault rupture models with constant super-shear rupture velocity. Geophys. J. Int. 162, 431–447. http://dx.doi.org/10.1111/j.1365-246X.2005.02611.x.

Bizzarri, A., 2010. How to promote earthquake ruptures: different nucleation strategies in a dynamic model with slip-weakening friction. Bull. Seism. Soc. Am. 100 (3), 923–940. http://dx.doi.org/10.1785/0120090179.

Bizzarri, A., 2011. On the deterministic description of earthquakes. Rev. Geophys. 49, RG3002. http://dx.doi.org/10.1029/2011RG000356.

Bizzarri, A., 2013. Energy flux of propagating ruptures with cohesive force. Bull. Seism. Soc. Am. 103 (5), 2670–2679. http://dx.doi.org/10.1785/0120120335.

Bizzarri, A., 2014a. The mechanics of seismic faulting: recent advances and open issues. La Rivista del Nuovo Cimento 37 (4), 181–271. http://dx.doi.org/10.1393/ncr/i2014-10099-0.

Bizzarri, A., 2014b. Rake rotation introduces ambiguity in the formulation of slip-dependent constitutive models: slip modulus or slip path? Ann. Geophys. 57 (5), S0547. http://dx.doi.org/10.4401/ag-6582.

Bizzarri, A., Cocco, M., 2005. 3D dynamic simulations of spontaneous rupture propagation governed by different constitutive laws with rake rotation allowed. Ann. Geophys. 48 (2), 279–299.

Bizzarri, A., Das, S., 2012. Mechanics of 3-D shear cracks between Rayleigh and shear wave rupture speeds. Earth Plan. Sci. Lett. 357–358, 397–404. http://dx.doi.org/10.1016/j.epsl.2012.09.053.

Bizzarri, A., Spudich, P., 2008. Effects of supershear rupture speed on the high-frequency content of S waves investigated using spontaneous dynamic rupture models and isochrone theory. J. Geophys. Res. 113, B05304. http://dx.doi.org/10.1029/2007JB005146.

Bizzarri, A., Cocco, M., Andrews, D.J., Boschi, E., 2001. Solving the dynamic rupture problem with different numerical approaches and constitutive laws. Geophys. J. Int. 144, 656–678.

Bizzarri, A., Dunham, E.M., Spudich, P., 2010. Coherence of Mach fronts during heterogeneous supershear earthquake rupture propagation: simulations and comparison with observations. J. Geophys. Res. 115, B08301. http://dx.doi.org/10.1029/2009JB006819.

Broberg, K.B., 1999. Cracks and Fracture. Academic Press, New York, p. 752.

Chen, X.-F., Zhang, H.-M., 2006. Modelling rupture dynamics of a planar fault in 3-D half space by Boundary Integral Equation Method: an overview. Pure Appl. Geophys. 163 (2), 267–299.

Das, S., 2007. The need to study speed. Science 317, 905–906. http://dx.doi.org/10.1126/science.1142143.

Das, S., Aki, K., 1977a. A numerical study of two-dimensional spontaneous rupture propagation. Geophys. J. Roy. Astr. Soc. 50, 643–668.

Das, S., Aki, K., 1977b. Fault plane with barriers: a versatile earthquake model. J. Geophys. Res. 82 (36), 5658–5670.

Day, S.M., Gonzalez, S.H., Anooshehpoor, R., Brune, J.N., 2008. Scale model and numerical simulations of near-fault seismic directivity. Bull. Seism. Soc. Am. 98 (3), 1186–1206.

Dunham, E.M., Archuleta, J.R., 2004. Evidence for a super-shear transient during the 2002 Denali fault earthquake. Bull. Seismol. Soc. Am. 94 (6B), S256–S268. http://dx.doi.org/10.1785/0120040616.

Dunham, E.M., 2007. Conditions governing the occurrence of supershear ruptures under slip-weakening friction. J. Geophys. Res. 112, B07302. http://dx.doi.org/10.1029/2006JB004717.

Dunham, E.M., Bhat, H.S., 2008. Attenuation of radiated ground motion and stresses from three-dimensional supershear ruptures. J. Geophys. Res. 113, B08319. http://dx.doi.org/10.1029/2007JB005182.

Festa, G., Vilotte, J.P., 2006. Influence of the rupture initiation on the intersonic transition: crack-like versus pulse-like modes. Geophys. Res. Lett. 33, L15320. http://dx.doi.org/10.1029/2006GL026378.

Fukuyaman, E., Madariaga, R., 1998. Rupture dynamics of a planar fault in a 3D elastic medium: rate- and slip-weakening friction. Bull. Seism. Soc. Am. 88 (1), 1–17.

Geubelle, P.H., Kubair, D.V., 2001. Intersonic crack propagation in homogeneous media under shear-dominated loading: numerical analysis. J. Mech. Phys. Solids 49 (3), 571–587.

Kaneko, Y., Lapusta, N., 2010. Supershear transition due to a free surface in 3-D simulations of spontaneous dynamic rupture on vertical strike-slip faults. Tectonophysics 493 (3), 272–284.

Kostrov, B.V., Das, S., 1988. Principles of Earthquake Source Mechanics. Cambridge Univ. Press, Cambridge, UK, p. 286.

Liu, C., Bizzarri, A., Das, S., 2014. Progression of spontaneous in-plane shear faults from sub-Rayleigh to compressional wave rupture speeds. J. Geophys. Res. Solid Earth 119. http://dx.doi.org/10.1002/2014JB011187.

Liu, Y., Lapusta, N., 2008. Transition of mode II cracks from sub-Rayleigh to intersonic speeds in the presence of favorable heterogeneity. J. Mech. Phys. Solids 56 (1), 25–50.

Lu, X., Lapusta, N., Rosakis, A.J., 2009. Analysis of supershear transition regimes in rupture experiments: the effect of nucleation conditions and friction parameters. Geopys. J. Int. 177 (2), 717–732.

Mello, M., Bhat, H.S., Rosakis, A., Kanamori, H., 2010. Identifying the unique ground motion signatures of supershear earthquakes: Theory and experiments. Tectonophysics 493, 297–326. http://dx.doi.org/10.1016/j.tecto.2010.07.003.

Mello, M., Bhat, H.S., Rosakis, A., Kanamori, H., 2014. Reproducing the supershear portion of the 2002 Denali earthquake rupture in laboratory. Earth Plan. Sci. Lett. 387, 89–96. http://dx.doi.org/10.1016/j.epsl.2013.11.030.

Olsen, K.B., Madariaga, R., Archuleta, R., 1997. Three-dimensional dynamic simulation of the 1992 Landers earthquake. Science 278, 834–838.

Spudich, P., Frazer, L.N., 1984. Use of ray theory to calculate high-frequency radiation from earthquake sources having spatially variable rupture velocity and stress drop. Bull. Seismol. Soc. Am. 74, 2061–2082.

Zhang, H.-M., Chen, X.-F., 2006. Dynamic rupture on a planar fault in three-dimensional half-space – II. Validations and numerical experiments. Geophys. J. Int. 167 (2), 917–932.

Zhang, Z., Zhang, W., Chen, X., 2014. Three-dimensional curved grid finite-difference modelling for non-planar rupture dynamics. Geophys. J. Int. 199, 860–879. http://dx.doi.org/10.1093/gji/ggu308.